arXiv:1703.01185v2 [astro-ph.HE] 26 Apr 2017

Synchrotron spectrum of fast cooling electrons in GRBs

Xiao-Hong Zhao[1,2,3], Jin-Ming Bai[1,2,3]

1. ABSTRACT

We discuss the synchrotron emission of fast cooling electrons in shocks. The fast cooling electrons behind the shocks can generate a position-dependent inhomogeneous electron distribution if they have not enough time to mix homogeneously. This would lead to a very different synchrotron spectrum in low frequency bands from that in the homogeneous case due to the synchrotron absorption. In this paper, we calculate the synchrotron spectrum in this inhomogeneous case in a gamma-ray burst (GRB). Both the forward shock and the reverse shock are considered. We find for the reverse shock dominated case, we would expect a "reverse shock bump" in the low frequency spectrum. The spectral bump is due to the combining synchrotron absorption in both the forward and reverse shock regions. In the forward shock spectrum in the low frequencies has two unconventional segments with spectral slopes of $\lesssim 1$ and 11/8. The slope of 11/8 has been found by some authors, while the slope of $\lesssim 1$ is new, which is due to the approximately constant electron temperature in the optically thick region. In the future, simultaneous observations in multiple bands (especially in the low frequency bands) in the GRB early afterglow or prompt emission phases will possibly reveal these spectral characteristics and enable us to identify the reverse shock component and distinguish between the forward and reverse shock emissions. This also may be as a method to diagnose the electron distribution status (homogeneous or inhomogeneous) after fast cooling in relativistic shock region.

2. INTRODUCTION

Gamma-ray bursts (GRBs) are the most powerful explosions in the universe. The standard fireball and internal-external shock models succeeded in explaining many observations,

[1]Yunnan Observatories, Chinese Academy of Sciences, 396 Yangfangwang, Guandu District, Kunming, 650216, P. R. China (e-mail: zhaoxh@ynao.ac.cn)

[2]Center for Astronomical Mega-Science, Chinese Academy of Sciences, 20A Datun Road, Chaoyang District, Beijing, 100012, P. R. China

[3]Key Laboratory for the Structure and Evolution of Celestial Objects, Chinese Academy of Sciences, 396 Yangfangwang, Guandu District, Kunming, 650216, P. R. China

especially the late GRB afterglow data. The internal shock model is one of the dominant models explaining the GRB prompt emission (Paczynski & Xu 1994; Rees & Mészáros 1994), although it suffers several crucial drawbacks (see Zhang & Yan 2011 for a summary). The traditional internal shock model involves an unsteady relativistic wind (or multiple shells) driven by the GRB central engine. A collision between two shells with different speeds would generate a forward shock and a reverse shock, in which the electrons are accelerated and produce the prompt emission.

After a series of collisions, the merged shell runs into the circumburst medium and will also generate a forward shock and a reverse shock (external shock) again. The forward shock (blast wave) model (Sari et al. 1998) is well consistent with the GRB afterglow data (e.g. Galama et al. 1998). However, the expected bright reverse shock emission in the early afterglow is not observed in the majority of bursts (Roming et al. 2006). Only a handful of bursts appear to be consistent with the reverse shock model (e.g. GRB 990123, Sari & Piran 1999, however, see Meszaros & Rees 1999 and Wei 2007, or recent bursts, GRBs 130427A and 160509A, Laskar et al. 2013, 2016). This can be because the shells from the central engine are magnetized and the reverse shock is not as strong as expected (e.g., Zhang & Kobayashi 2005; Fan, Wei & Wang 2004). The complexity of the reverse shock emission (e.g. Kobayashi 2000 and Wu et al. 2003) and its superposition with the forward shock emission also makes the identification of the reverse shock signature from the light curve difficult.

In GRB prompt and early afterglow phases, the magnetic field in the emission regions is strong enough that the energetic electrons accelerated in the shocks cool by synchrotron or inverse Compton radiations within a much shorter time scale than the dynamic time[1], which is called fast cooling. The spectrum in the fast cooling regime for a homogeneous electron distribution has been studied detailedly by some authors (e.g., Sari et al. 1998). The spectral slope below the synchrotron-self absorption (SSA) frequency is 2 or 5/2. However, because electrons in the shocked shell are accelerated instantaneously and then cool before the shock crosses through the shell, the electron with different (equivalent) temperatures can have not enough time to diffuse throughout the shell and thus the electrons distribution is position-dependent, i.e, the electron distribution in the shell can be inhomogeneous. The inhomogeneity will considerably affect the spectrum below the synchrotron absorption frequency. Granot et al. (2000) have found the spectrum has an unconventional segment with a slope of 11/8 in this case. We will show in the later sections that their result is for the forward shock.

[1]Here the dynamic time is the time in which the shock crosses through the shell.

As we know that the forward shock and the reverse shock would be produced in pairs. If the forward shock is advancing toward us, the reverse shock emission would cross through the forward shock region before it reaches us. This can affect the reverse shock spectrum significantly if the forward shock is optically thick to the reverse shock emission at low frequencies. Thus both shocks need to be considered when the emission from the two regions are considered. Here we revisit the inhomogeneity problem and consider both the reverse shock and forward shock. We find some unprecedented spectral characteristics. This paper is organized as follows. In section 3, we derive the electron distribution in the inhomogeneous case. Section 4 is the calculation of the synchrotron emission. In the last section, we discuss the possible application of our results.

3. MODELS

When a shock is crossing a shell, the electrons in a very thin layer (fluid element) behind the shock will be accelerated instantaneously into a power-law distribution. With the shock crossing the shell, more fluid elements become hot and cool down rapidly by synchrotron and inverse Compton (IC) radiation. These fluid elements have different electron equivalent temperatures due to the electrons accelerated at different times. This would generate a temperature gradient: the electrons near the shock front have not enough time to cool down but still remain hot while those far downstream would be cooler.

3.1. ELECTRON DISTRIBUTION STRUCTURE

Fig. 1 is the schematic of electron status in the forward and reverse shock regions. The equivalent temperatures in low frequency regions (the red region and the purple red regions in Fig. 1) in the two shocks can be different due to different electron number densities. We consider the time when the reverse shock right crosses through the shell and a photon is emitted from the reverse shock front. At this time, the reverse shock emission reaches its peak. With the traveling of the photon in the shocked shell toward the observer, more photons along the photon path in the shell will be emitted and encounter absorption during their propagation.

We can define several critical positions behind shock front in each shocked region. The first is x_m. All the electrons within the fluid element at x_m cool down to $\sim \gamma_m$ due to the radiation loss. The radiation power is $P_r = \frac{4}{3}\sigma_T c(\gamma_e^2 - 1)U_B(1 + Y)$ including the cyclo-synchrotron and IC radiations, where Y is the Compton Y factor and $U_B = B^2/8\pi$ is the

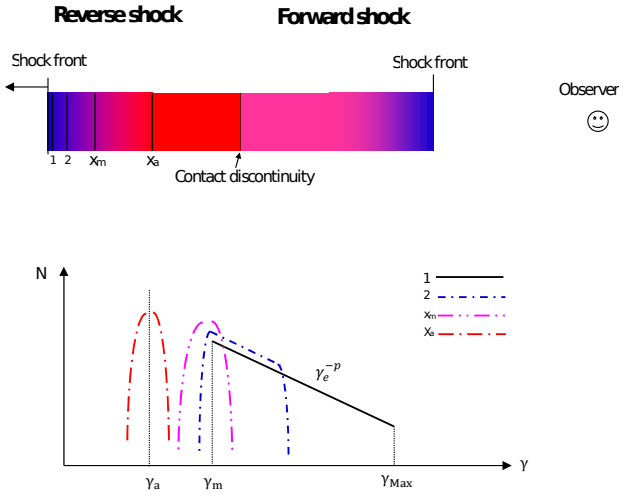

Fig. 1.— Schematic of the equivalent temperature and the electron distribution in shocked shells. The color bar from blue to red in the upper part indicates the equivalent temperatures of the shells from hot to cool. Positions 1, 2 have different electron distributions due to different distances from the shock front and the corresponding electron distributions are shown in the lower part of this picture. x_m is the position where all the electrons cool down to $\sim \gamma_m$. x_a is the position where the synchrotron peak frequency of electrons is equal to $\hat{\nu}_a$. See the text.

comoving magnetic field energy density. c and σ_T are the light speed and the Thomson cross section, respectively. Below x_m, the electrons at the fluid elements are hot and approximately remain a power law distribution with a high energy cutoff at some energy of $\hat{\gamma}_c$, while beyond it, most electrons begin to cool (below γ_m) and approximately have a monoenergetic distribution with an energy of $\hat{\gamma}_c$. Here $\hat{\gamma}_c$ is the energy to which the electrons cool down since the shock front passes some given position x behind the shock front:

$$\hat{\gamma}_c(x) = \frac{1 + e^{-2bt(x)}}{1 - e^{-2bt(x)}} \tag{1}$$

where $b = 4\sigma_T U_B(1+Y)/3m_e c$ is a factor and m_e is the electron mass. t is the elapsed time since the electrons at x are accelerated. Here the form of $\hat{\gamma}_c$ can apply to both the ultrarelativistic and non-relativistic cases. When $2bt \ll 1$, which corresponds to the ultra-relativistic case, we go back to the familiar form $\hat{\gamma}_c = 6\pi m_e c/\sigma_T B^2(1+Y)t$. The time t can be given by

$$t(x) = \begin{cases} 4x/c & \text{reverse shock region} \\ (6\Delta - 2x)/c & \text{forward shock region.} \end{cases} \tag{2}$$

We take into account the relativistic shock speed of $c/3$ in the shocked shell frame. In GRB, the internal shock is mildly relativistic for typical parameters and thus the shock speed in the shocked shell would be $\lesssim c/3$, which may somewhat affect the final result. Δ is the comoving width of the shell.

The Compton Y factor is defined by the ratio of synchrotron photon energy density, including the contributions from the reverse shock region ($U_{syn,rs}$) and the forward shock region ($U_{syn,fs}$), to the magnetic field energy density, i.e., $Y \equiv (U_{syn,rs} + U_{syn,fs})/U_B = [-1 + \sqrt{1 + 4(U_{e,rs} + U_{e,fs})/U_B}]/2$ (Sari & Esin 2001). $U_{e,rs}$ and $U_{e,fs}$ are the electron energy densities in the two shocked regions. The corresponding electron number densities are $n_{0,rs}$ and $n_{0,fs}$. We neglect the second IC scattering, since it should occur in the Klein-Nishina limit. Note that in the shock case, though the electron distribution can be inhomogeneous due to insufficient diffusion time, the photon energes are approximately homogeneously distributed in the shocked shell because of the transparency of the shell to the spectral peak energy (ν_m, synchrotron peak frequency corresponding to γ_m). Thus we have $(U_{e,rs} + U_{e,fs})/U_B \simeq [(p-1)/(p-2)]m_e c^2 (n_{0,rs} + n_{0,fs})\gamma_m/U_B$. Here we assume the heated electrons in the shocked regions have the distribution of $dN/d\gamma_e \propto \gamma_e^{-p}$ and p is the electron power-law slope.

The second critical position is x_a. As mentioned above, in the cool part of the shocked shell, the electrons in each fluid element have approximately mono energy distributions. There is a position where the synchrotron peak frequency of electrons is equal to a frequency $\hat{\nu}_a$ at which the optical depth is equal to 1. x_a can be obtained by solving

$$\int_0^{x_a} \alpha_\nu(x, \hat{\nu}_a) dx = 1, \tag{3}$$

where α_ν is the absorption coefficient and will be given in the next section, $\hat{\nu}_a = 0.45 q_e B \hat{\gamma}_a^2/2\pi m_e c$ is used and $\hat{\gamma}_a$ is the electron energy corresponding to $\hat{\nu}_a$. Over x_a, the electrons begin to be thermalized with the peak of $\hat{\gamma}_a$ and the peak energy approximately remains a constant. An alternative derivation of $\hat{\nu}_a$ and $\hat{\gamma}_a$ is by balancing the cooling and SSA heating, which should give similar results for $p < 3$ (Ghisellini & Svensson 1989). We calculate $x_{a,rs}$ ($\hat{\gamma}_{a,rs}$) and $x_{a,fs}$ ($\hat{\gamma}_{a,fs}$) independently in the reverse and forward shock regions, respectively, using the assumption that the radiation in one region does not affect the electron equivalent temperature in the other region.

We now can give the approximate electron distribution at each fluid element in the shocked shell:

$$\frac{dN(x)}{d\gamma_e} \simeq \begin{cases} \frac{n_0(p-1)}{\gamma_m}(\frac{\gamma_e}{\gamma_m})^{-p}(1 - b\gamma_e t)^{p-2} & \gamma_m < \gamma_e < \hat{\gamma}_c(x) \quad \text{or} \quad 0 < x < x_m \\ n_0 \delta[\gamma_e - \hat{\gamma}_c(x)] & \hat{\gamma}_a < \gamma_e \leq \gamma_m \quad \text{or} \quad x_m \leq x \leq x_a \\ n_0 \delta[\gamma_e - \hat{\gamma}_a] & \gamma_e \leq \hat{\gamma}_a \quad \text{or} \quad x_a < x \leq \Delta, \end{cases} \tag{4}$$

where n_0 is the electron number density. The first equation describes the evolution of the instantaneously injected electrons with a power-law electron distribution (Kardashev 1962). The electron distribution in the region larger than x_m in the shell are described by a δ-function. In the region larger than x_a, the electron cooling by radiation is ineffective due to the balance between the SSA heating and the synchrotron+IC cooling and thus the electron peak energy roughly remains a constant until the electrons cool by adiabatic expansion. Here we neglected the escape of electrons, since the electrons should be confined by the magnetic field within a dynamic time scale.

3.2. SYNCHROTRON SPECTRUM

Using the above electron distribution, we can derive the synchrotron intensity I_ν. The emission and absorption coefficients at each fluid element can be given by

$$j_\nu = \begin{cases} \frac{1}{4\pi}\int d\gamma_e N P_\nu & \hat{\gamma}_c \geq \gamma_m \\ \frac{N_0}{4\pi} P_\nu(\hat{\gamma}_c) & 2 < \hat{\gamma}_c < \gamma_m \\ \frac{N_0}{4\pi} P_{\nu,cyc} & \hat{\gamma}_c < 2 \end{cases} \tag{5}$$

$$\alpha_\nu = \begin{cases} -\frac{1}{8\pi m_e \nu^2}\int d\gamma_e \gamma_e p_e P_\nu \frac{\partial}{\partial \gamma_e}\left(\frac{N}{\gamma_e p_e}\right) & \hat{\gamma}_c \geq \gamma_m \\ \frac{N_0}{8\pi m_e \nu^2 \hat{\gamma}_c^2}[\frac{d}{d\gamma_e}(\gamma_e^2 P_\nu)]_{\gamma_e=\hat{\gamma}_c} & 2 < \hat{\gamma}_c < \gamma_m \\ \frac{N_0}{8\pi m_e \nu^2 \hat{\gamma}_c p_c}[\frac{d}{d\gamma_e}(\gamma_e p_e P_{\nu,cyc})]_{\gamma_e=\hat{\gamma}_c} & \hat{\gamma}_c \leq 2, \end{cases} \tag{6}$$

where P_ν is the synchrotron spectral power and $P_{\nu,cyc} = \frac{4\sigma_T c}{3\pi}\frac{p_c^2 U_B}{\nu_L}\frac{2}{1+3p_c^2} e^{-\frac{2(1-\nu/\nu_L)}{1+3p_c^2}}$ is the approximate cyclo-synchrotron power spectrum and applies to electron energy < 2 (Ghisellini et al. 1998). $p_c = \sqrt{\hat{\gamma}_c^2 - 1}$ and $p_e = \sqrt{\gamma_e^2 - 1}$ are the electron momentums, and ν_L is the Larmor frequency. In the above second formula, we can find the absorption coefficient decreases with a power law of $\nu^{-5/3}$ below the synchrotron peak frequency $\nu(\hat{\gamma}_c)$, while it exponentially decreases over it. Thus the synchrotron absorption optical depth in a region with a given electron energy considerably decreases with the photon frequency increase when the photon frequency is higher than the synchrotron peak frequency the electron emits.

We can give the radiation intensity based on the radiative transfer equation:

$$I_\nu = \int_0^\Delta j_{\nu,rs} e^{-\int_x^{3\Delta}\alpha_{\nu,rs}ds} dx + \int_\Delta^{3\Delta} j_{\nu,fs} e^{-\int_x^{3\Delta}\alpha_{\nu,fs}ds} dx \tag{7}$$

Here the upper limit of Δ corresponds to the peak time of the reverse shock emission in the observer frame. The subscripts fs and rs denote the forward shock and the reverse

shock, respectively. The right terms of the equation are composed of two parts including the contribution of the reverse and the forward shock regions. We take into account the fact that the reverse shock emission would cross through both the reverse and forward shock regions before it reaches the observer. The upper limit of 3Δ is due to the fact that when the reverse shock emission catches up with the forward shock front, it travels 3Δ in the shocked shell (or medium) frame. We focus on the *relativistic* reverse shock in the paper, which has stronger emission compared with the Newton reverse shock, and we can neglect the shell spreading.

4. RESULTS

The spectral calculation depends on many unknown shock parameters. The parameters in GRB and its afterglow can be in a wide range. We first calculate the spectra by adopting parameters in wide range. Then we take a group of plausible parameters in afterglow and calculate the spectrum.

4.1. GENERAL PARAMETERS

Fig. 2-4 indicate the resulting spectra and the spectral slopes (in the comoving frame of the shocked shell). One can find that the reverse shock spectrum has a bump when the electron number density in the reverse shock region is much larger than that in the forward shock region. This is because the photons from the reverse shock region encounter the absorptions in both the forward and reverse shock regions. The synchrotron absorption from the forward shock region would lead to a sharp cutoff toward low frequencies due to the exponential increase of the optical depth with frequency decrease. In low frequencies below the cutoff, the spectrum would be dominated by the forward shock emission. With the increase of the photon frequency, the forward shock region gradually becomes optical thin to the reverse shock emission. The reverse shock emission will generate a bump due to the piling-up of electrons at around $\hat{\gamma}_{a,rs}$. When the photon frequency is high enough that the whole shell is transparent, the spectrum goes back to the optical-thin case.

When the electron density of the forward shock region is much larger than that in the reverse shock region, the forward shock emission is dominated. The forward shock spectrum is quite different compared with the conventional homogeneous case. There is an unconventional spectra segment in the low frequency bands, with a slope of 11/8, which has been found by Granot et al. (2000). This segment results from the equivalent temperature gradient in the shocked shell. The lower the photon frequency, the more approaching the

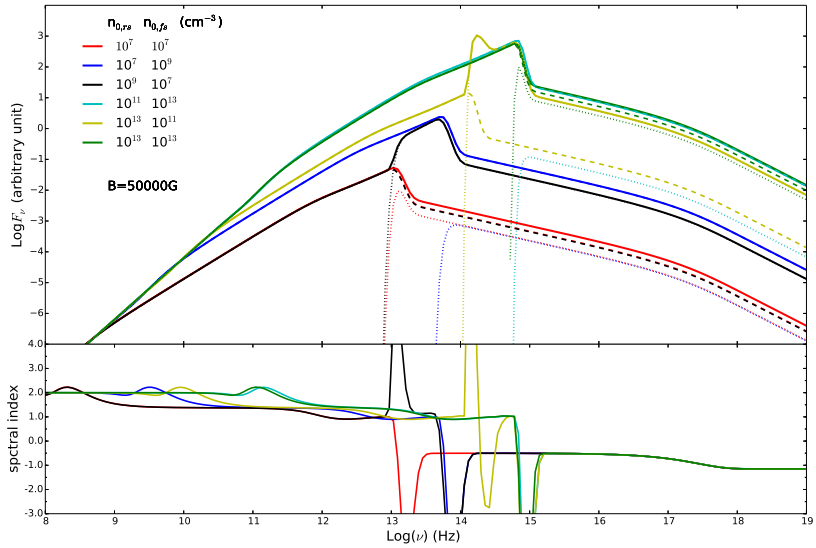

Fig. 2.— The spectra (the upper panel) and the corresponding spectral index (lower panel) with the magnetic field of $B = 5 \times 10^4$ G. Different colors represent different parameters, marked in the figure. Other parameters are γ_m=10^3,γ_{Max}=10^7, p=2.3 and Δ=10^{12}cm. In the upper panels, the solid lines represent the spectra from the shocked regions. The dotted lines and the dashed lines represent the contributions from the reverse shock and the forward shock, res

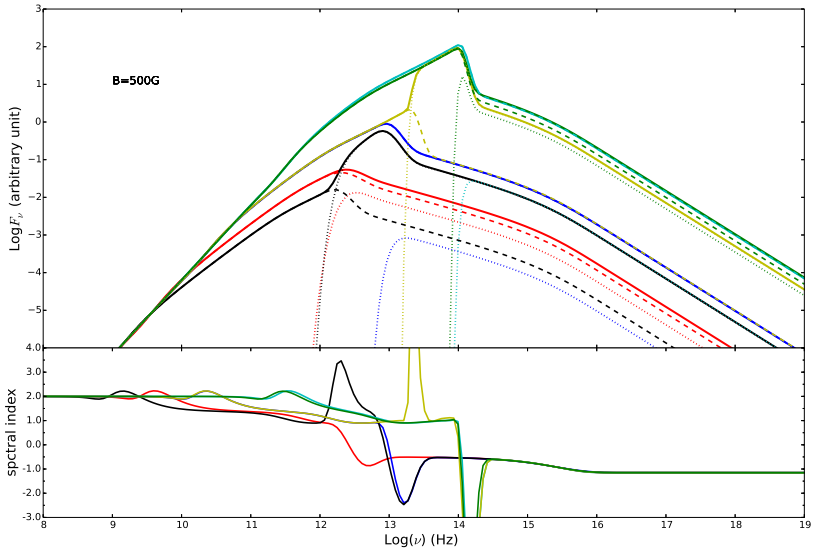

Fig. 3.— Same as in Fig. 2 but for the magnetic field of $B = 500$ G.

forward shock front the emitted position. When the emitted position is close enough to the shock front, electrons would be uncooled (with the average energy of $\sim \gamma_m$) and thus the

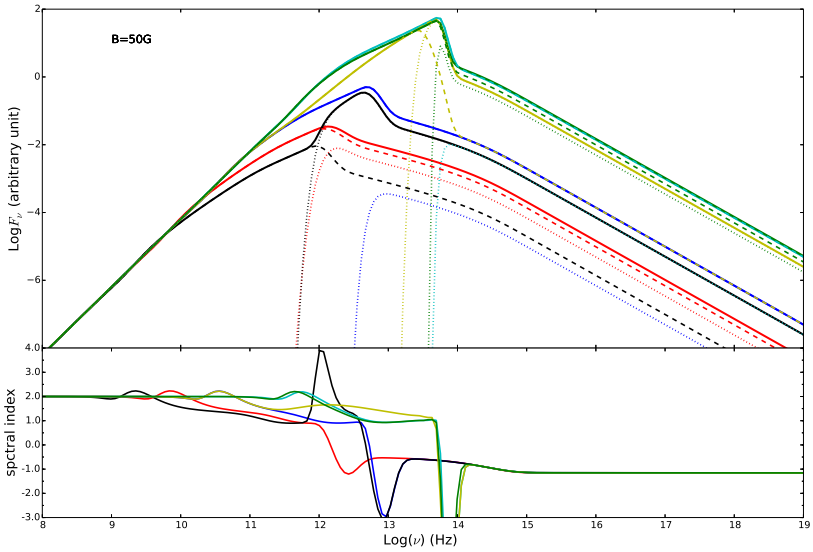

Fig. 4.— Same as in Fig. 2 but for the magnetic field of $B = 50$ G and shell width of $\Delta = 10^{13}$cm.

spectral slope would be 2 due to the absorption mainly from the electrons of γ_m. Another segment has a spectral index of ~ 1, which is a new segment. This segment is due to the fact that with the frequency increase, the electrons with the dominated contribution to the emission come to the SSA region (larger than $x_{a,fs}$) and the electron number approximately linearly increase with the frequency, which leads to a spectrum with a slope of ~ 1. It is worth noting that the segment of ~ 1 also appears in the reverse shock spectrum around the bump, which is due to the contributions of electrons in the reverse shock SSA region.

4.2. APPLICATION TO THE EARLY AFTERGLOW

We present an application of our model in early afterglow in this section. The circumburst environment in GRBs is usually believed to be stellar wind (Chevalier & Li 2000) or interstellar medium (ISM). Here we consider the wind case (Wu et al. 2003). Using a group of plausible parameters for GRB afterglows, we calculate the spectrum when the reverse shock just crosses the shell. The number densities in the reverse and forward shock regions are $n_{0,rs} = 2.1 \times 10^9 \mathrm{cm}^{-3} (\frac{A}{3\times10^{35}})^{5/4} E_{52}^{-1/4} (\frac{\Gamma}{300})^{3/4} \Delta_{14}^{-7/4}$ and $n_{0,fs} = 6.9 \times 10^7 \mathrm{cm}^{-3} (\frac{A}{3\times10^{35}})^{7/4} E_{52}^{-3/4} (\frac{\Gamma}{300})^{5/4} \Delta_{14}^{-5/4}$, respectively. Here the circumburst number density profile is $n = Ar^{-2}$, where $A = \dot{M}/4\pi m_p v_w = 3 \times 10^{35} \mathrm{cm}^{-1} (\dot{M}/10^{-5} M_\odot \mathrm{yr}^{-1}) (v_w/10^3 \mathrm{km\ s}^{-1})^{-1}$. E and Γ are the energy and the initial Lorentz factor of the shell, respectively. We use the usual notation $Q = 10^m Q_m$ throughout the paper. Assuming the magnetic field

energy fraction of the internal energy ϵ_B in the two regions are the same, then the magnetic fields in the two regions are also the same, which are given by $B = \sqrt{8\pi e_{fs}\epsilon_B} = 1883.1$ G$(\frac{A}{3\times10^{35}})^{3/4}E_{52}^{-1/4}(\frac{\Gamma}{300})^{3/4}\Delta_{14}^{-3/4}\epsilon_{B,-2}^{1/2}$ and $e_{fs} = 1.4\times10^7$ erg cm$^{-3}(\frac{A}{3\times10^{35}})^{3/2}E_{52}^{-1/2}(\frac{\Gamma}{300})^{3/2}\Delta_{14}^{-3/2}$ is the internal energy density in the two shocked region. The Lorentz factor of the shocked shell and medium is $\gamma_{sh} = 33.9(\frac{A}{3\times10^{35}})^{-1/4}E_{52}^{1/4}(\frac{\Gamma}{300})^{1/4}\Delta_{14}^{-1/4}$. The minimum Lorentz factors in the two regions are $\gamma_{m,rs} = \epsilon_e(\bar{\gamma}_{rs} - 1)[(p-2)/(p-1)]m_p/m_e = 144.8$, where $\bar{\gamma}_{rs} = 4.4(\frac{A}{3\times10^{35}})^{1/4}E_{52}^{-1/4}(\frac{\Gamma}{300})^{3/4}\Delta_{14}^{1/4}$ is the Lorentz factor of shocked shell relative to the unshocked shell and $\epsilon_e = 0.1$ is the electron energy fraction of the internal energy, and $\gamma_{m,fs} = \epsilon_e\gamma_{sh}[(p-2)/(p-1)]m_p/m_e = 1392.6$. The resulting spectrum is shown in Fig.5. We can find the reverse shock flux begins to exceed the forward shock flux from around 4×10^{14} Hz. At V band ($\sim 5.4\times10^{14}$ Hz), the reverse shock flux is roughly one order of magnitude higher than the forward shock flux, i.e., the reverse shock emission is brighter than the forward shock emission by ~ 2.5 mag at V band. The reverse shock spectral bump and the forward shock spectral segments of 11/8 and ~ 1 clearly appears. The bump lies between the UV and soft X-ray bands and seemingly will not be straightforward to observe. However, here we use some canonical parameters. In reality, GRB parameter ranges can be wide so that the reverse shock bump will also lie in a wide range. Thus the bumps for some bursts will possibly move to the observable bands, such as optical bands.

5. DISCUSSION

In this paper, we consider the case that the electron distributions in shocks in GRB and its early afterglow phases are inhomogeneous due to the fast cooling of the electrons. We calculate the spectra in this case by considering the radiative transfer. We find the spectrum in the optically thick part is quite different from that of the usually considered homogeneous case. For the reverse shock dominated case, the spectrum has a bump due to the combining absorption of the reverse and forward shock regions. For the forward shock dominated case, there is an unconventional slope of 11/8 in the spectrum, which is consistent with Granot et al. (2000 or Granot & Sari 2002). There is also a new spectral segment of ~ 1 following the segment of 11/8 toward high frequencies. Thus the spectral slopes of the forward shock emission for the fast cooling are (2,11/8,1,-1/2,-p/2) from low frequency to high frequency. We also present an application to the GRB early afterglow phase, i.e., the early forward and reverse shock phase of the external shock, with typical parameters. We find the above spectral characteristics, such as the reverse shock bump and the forward shock spectral segments of 11/8 and ~ 1, are all present. Such spectrum characteristics will possibly be observed in the future. It should be noted that such spectrum shape also possibly presents in other objects with similar physical conditions to GRBs, such as active

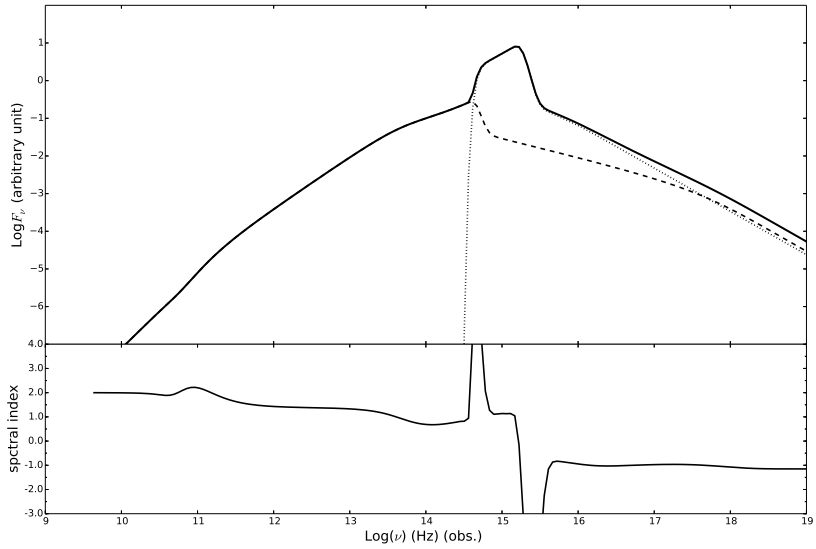

Fig. 5.— The synchrotron spectrum for typical parameters at early afterglow phase in the wind environment. We use the frequency in the observer frame taking into account the relativistic motion of the shocked material. The adopted parameters are E=10^{52} erg, A=3×10^{35}cm^{-1}, Γ=300, Δ=10^{14}cm, $p = 2.3$, $\epsilon_B = 0.01$ and $\epsilon_e = 0.1$. In the upper panel, the solid line represents the spectra from the shocked regions. The dotted line and the dashed line represent the contributions from the reverse shock and the forward shock, respectively. The spectral slope is shown in the lower panel.

galactic nuclei (AGNs).

Actually, the reverse shock signature of the external shock is not clearly confirmed to date from the data. Even the widely believed reverse shock cases, such as optical flashes of GRB 990123 and GRB 041219a, are still under debate. Mészáros & Rees (1999) and Wei (2007) considered the applicability of the internal shock model. As shown in this paper, the reverse shock emission has very distinct features and behaviors as a bump above the forward shock emission if it dominates over the forward emission, which is easily recognized. Thus this will be a method to identify the reverse shock emission from the spectrum. In the future if we observe the continuous spectrum in wide bands, especially in the low frequency bands at early afterglow phase, or even several uncontinuous points in the low frequency bands, we could find the reverse shock emission. While if the slopes of 11/8 and/or ~ 1 are observed, the spectrum should be from the forward shock.

If such spectra are detected in the prompt emission phase, this suggests that the prompt emission should come from a shock, most possibly the internal shock. The shock model can naturally generate such an inhomogenity we discuss in the paper. This may be used to

distinguish between the internal shock model and other dissipation models, such as the magnetic reconnection model (e.g., Zhang & Yan 2011) where the electron distribution is close to the homogeneous case, since the magnetic reconnection occurs randomly.

Such spectral observation in turn suggests the electron distributions in shocks are indeed inhomogeneous, which may also present us new insight into the diffusing process of fast cooling electrons behind a relativistic shock. The diffusion process of electrons is not well understood in physics, depending on some unknown factors such as magnetic field strengthen and structure in the emission region, which requires more MHD simulation of shock. On the contrary, if the spectrum is characterized by the slopes like 2 and/or 5/2 in low frequencies, then this may suggest the electron distribution of the emission region is homogeneous. Thus the spectrum observation will be a probe of the mixability of electron distribution in emission region.

In observations, the wide band detections at early times, thanks to the rapid localization of GRBs by swift, have given us unprecedented insight into GRB early afterglow physics (e.g., Zhang et al. 2006), though the coverage of bands is not enough to give us the spectral information yet. However, the follow-up projects, especially in the low energies, are increasing. The GRB and its early afterglow spectral detection in wider bands than now is promising. SVOM (Paul et al. 2011; Wei et al. 2016), NGRG (Grossan et al. 2014) and UFFO (Grossan et al. 2012; Park et al. 2013) will allow simultaneous or rapid follow-up observations of GRB in wide bands. GWAC (the Ground Wide Angle Camera) will possibly observe the optical emission and GFTs (the Ground follow-up Telescope) will observe the near infrared emission during, after or even before GRBs (Paul et al. 2011). Early observations in longer wavelengths, such as millimeter band and submillimeter band can be operated by EVLA (the Expanded very large Array [2]) or ALMA (the Atacama Large Millimeter/submillimeter Array [3]). SKA (the Square Kilometer Array, e.g., Carilli et al. 2003) and FAST (the Five-Hunfred Aperture Spherical Radio Telescope, Nan et al. 2011) will possibly contribute to the radio observation. All these instruments will provide us more spectral information at the early afterglow time or even during the GRB, allowing us to diagnose the revers shock and the forward shock signatures.

We thank Z. Li and X. F. Wu for useful suggestions and comments. We also thank an anonymous referee for valuable comments to improve the paper. We acknowledge partial support by the Chinese Natural Science Foundation (No. 11203067, 11133006, 11433004),

[2]http://www.aoc.nrao.edu/evla/

[3]http://www.almaobservatory.org

Yunnan Natural Science Foundation (2011FB115 and 2014FB188) (X.H.Z.) and the Key Research Program of the CAS (Grant NO. KJZD-EW-M06) (J.M.B.).

REFERENCES

Carilli, C. L., Ivison, R. J., & Frail, D. A. 2003, ApJ, 590, 192

Chevalier, R. A., & Li, Z.-Y. 2000, ApJ, 536, 195

Fan, Y. Z., Wei, D. M., & Wang, C. F. 2004, A&A, 424, 477

Galama, T. J., Wijers, R. A. M. J., Bremer, M., et al. 1998, ApJ, 500, L97

Ghisellini, G., & Svensson, R. 1990, ASIC, 305, 395

Ghisellini, G., Haardt, F., & Svensson, R. 1998, MNRAS, 297, 348

Granot, J., Piran, T., & Sari, R. 2000, ApJ, 534, L163

Granot, J., & Sari, R. 2002, ApJ, 568, 820

Grossan, B., Park, I. H., Ahmad, S., et al. 2012, Proc. SPIE, 8443, 84432R

Grossan, B., Kumar, P., Perley, D., & Smoot, G. F. 2014, PASP, 126, 885

Kardashev, N. S. 1962, Soviet Ast., 6, 317

Kobayashi, S. 2000, ApJ, 545, 807

Laskar, T., Berger, E., Zauderer, B. A., et al. 2013, ApJ, 776, 119

Laskar, T., Alexander, K. D., Berger, E., et al. 2016, ApJ, 833, 88

Mészáros, P., & Rees, M. J. 1999, MNRAS, 306, L39

Nan, R., Li, D., Jin, C., et al. 2011, International Journal of Modern Physics D, 20, 989

Paczynski, B., & Xu, G. 1994, ApJ, 427, 708

Park, I. H., Brandt, S., Budtz-Jørgensen, C., et al. 2013, New Journal of Physics, 15, 023031

Paul, J., Wei, J., Basa, S., & Zhang, S.-N. 2011, Comptes Rendus Physique, 12, 298

Rees, M. J., & Meszaros, P. 1994, ApJ, 430, L93

Roming, P. W. A., Schady, P., Fox, D. B., et al. 2006, ApJ, 652, 1416

Sari, R., & Esin, A. A. 2001, ApJ, 548, 787

Sari, R., & Piran, T. 1999, ApJ, 517, L109

Sari, R., Piran, T., & Narayan, R. 1998, ApJ, 497, L17

Wei, D. M. 2007, MNRAS, 374, 525

Wei, J., Cordier, B., Antier, S., et al. 2016, arXiv:1610.06892

Wu, X. F., Dai, Z. G., Huang, Y. F., & Lu, T. 2003, MNRAS, 342, 1131

Zhang, B., & Kobayashi, S. 2005, ApJ, 628, 315

Zhang, B., Fan, Y. Z., Dyks, J., et al. 2006, ApJ, 642, 354

Zhang, B., & Yan, H. 2011, ApJ, 726, 90

This preprint was prepared with the AAS LaTeX macros v5.2.